ICAS 2020 SHANG HAI
International Council of the Aeronautical Sciences
32nd Congress of the International Council of the Aeronautical Sciences
September 6-10, 2021
Pudong Shangri-La, Shanghai, China

ANALYTICAL MODELLING OF A HOVERABLE X-SHAPE FLAPPING WING AIRCRAFT CONSIDERING WING-TAIL INTERACTION

Zhao Longfei[1], Wang Wenshuo[2], Chen Yuxin[3] & Jiao Zongxia [4]

[1]Beihang University, Research Institute for Frontier Science
[2] Beihang University, School of Automation Science and Electrical Engineering
[3] Beihang University, School of Aeronautic Science and Engineering
[4] Beihang University, Ningbo Institute of Technology

Abstract

The topic of this study comes from hovering control requirement of a 0.8kg X-shape flapping wing aircraft. Due to relatively large scale and inertia than existing flapping wing vehicles, existing flapping wing vector control techniques are not convenent to be adopted. Instead, two tail control surfaces that work as elevon and a yaw control tail rotor are utilized. While flapping wing and rotor thrust force moddels are adequate, study related to tail control moddels is very scarce, especially those concentrate on slow or hovering flight, at which conditions the flapping wing induced flow plays a significant role in attitude control force generation. Therefore, this study concentrate on the control features and moddelling of the tail considering wing-tail interaction. New generation meshless numerical method is utilized and based on which the transient and cycle-averaged flow structure and aerodynamic force of the tail are analyzed. An analytical tail control force model is finally proposed.

Keywords: wing-tail interaction, flapping wing, hoverable, X-shape

1. Introduction

Flapping flight is the most common flight pattern among flying creatures [1]. Bionic flapping aircraft adopted this flight pattern, relying on a pair of flapping wings to generate thrust and lift at the same time, thus achieve stable flight without independent propulsion unit [2-5]. Compared with conventional fixed wing or rotor wing aircraft, flapping wing aircraft featured with low noise, high maneuverability, and strong environment adaptation[1, 6]. Excellent progress have been made in recent years in field of flapping structures [2, 7], fluid mechanisms [8-10], dynamic modelling [11-13] and control strategy [14-16], especially in NAV scale, within which flapping wings is believed to possess higher aerodynamic efficiency and to have more potential practicability than conventional aircraft layouts [1, 8, 17-19]. However, due to limited flight range, stability and mission capability, there seems a long way to put these insect-scale flapping wing aircrafts into practical. Nevertheless, bird scale flapping wing aircrafts are capable of utilizing mature high performance motors, batteries, control units, and various mission payloads, which are believed to achieve practical application in very near future [2, 20]. To this end, Beihawk, a hoverable 0.8kg X-shape wing flapping aircraft has been designed, which is capable of vertical takeoff and landing, taking over 200g payloads, and achieve at least 10min cruising flight. Conventional control surfaces are installed within the flapping induced flow field for attitude control. During VTOL(vertical takeoff and landing), when incoming flow speed is near zero, the attitude control force generation is fully rely on flapping wing induced flow. Although aerodynamic features of flapping wing itself is well studied, effective analysis tools of the impact of flapping wing wake on tail control surfaces that installed within induced flow field is still absent. The present study mainly focuses on the aerodynamic mechanism and dynamic model construction of tail control surfaces. An analytical semi-experimental aerodynamic model is derived. Relative conclusions is beneficial to aerodynamic and control design of control surfaces installed within flapping wing induced flow.

2. Layout of Beihawk

As illustrated in Fig.1, Beihawk has 1.2m wingspan and 0.8kg in weight, which is much heavier than existing hoverable ornithopters. To generate enough lift to balance the weight, clap-fling X-shape wing configuration is utilized to maximize power density, similar with Mentor [21] and Delfly [22]. Due to symmetry of flap motion to this plane, the wing induced flow near *x-o-z* where clap happens are constrained in the thrust direction. As a result, the otherwise propulsion efficiency loss owing to non-thrust-direction induced velocity is eliminated. The flapping frequency during hover is measured as around 8Hz. The wings are driven by a spatial crank-rocker mechanism. In order to decrease drag during level flight, the gears are arranged parallel with fuselage longitudinal section to achieve a smaller fuselage cross section area. Beihawk has four control channels including throttle, rudder propeller, and two channels for elevon. Throttle is realized by adjusting motor speed controller, by which the flapping frequency is capable of varying between 0-10Hz. Aileron are realized by two tail control surfaces installed on clap-fling plane, downstream of flapping wings, thus soaked in the strong axial induced wake to strengthen the control effect. Same polarity movement of the two surfaces generates pitch torque and different polarity deflection generates roll torque. Due to the gap of induced flow near the *x* axis, a control surface won't work in hovering at the position of a traditional vertical tail. Therefore, a two-way controllable tail propeller set was installed to actively generate yaw torque, similar as a normal helicopter tail rotor.

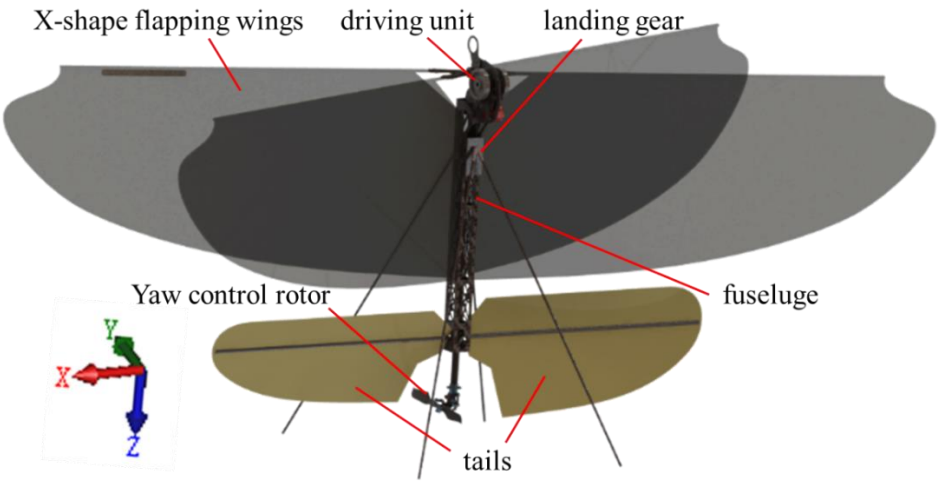

Fig. 1 Schematic of Beihawk flapping wing aircraft

3. Simulation setup

In this study, the interactional aerodynamic features between flapping wing and elevon are analyzed by numerical simulation. LBM(lattice Boltzmann method) is applied using a commercial LBM code: Next Limit Technologies' XFlow, which is specifically designed for applications in situations of highly transient flow fields and models with large-amplitude moving parts [23, 24]. To simulate the continuous spanwise twisting of a physical flapping wing, the wing surface is separated into six kinematic-independent blades, as illustrated in Fig. 2. Each wing blade is set as a flat thin plate having a thickness of 1 mm. The leading edge of each wing blade is collinear, and each blade plunges around the wing-root axis synchronously. The accuracy and robustness of such kinematic approximation method for flapping wing aerodynamic force, torque, and wake structure simulations has been demonstrated by previous study. The wing kinematic regularity is preset based on previous study by Jiao [24] and Gursul [9], assuming sine flapping angle and twisting angle within a flap cycle, arctangent twisting angle distribution along span-wise, and varying phase lag between flapping and twisting angle at specific flapping frequency. The simulational model layout is illustrated in Fig. 1, the kinematic constrains of each wing blade element are expressed as

$$\begin{cases} \phi(t) = 0.13\sin(2\pi ft + \dfrac{\pi}{2}) - 0.13 \\ \alpha_{t,n} = -\arctan(\dfrac{n}{6}\tan(\alpha_{t,\max}))\cos(2\pi ft + \beta_{\text{twist}}) \end{cases} \quad n = (1,\ldots,6) \quad . \tag{1}$$

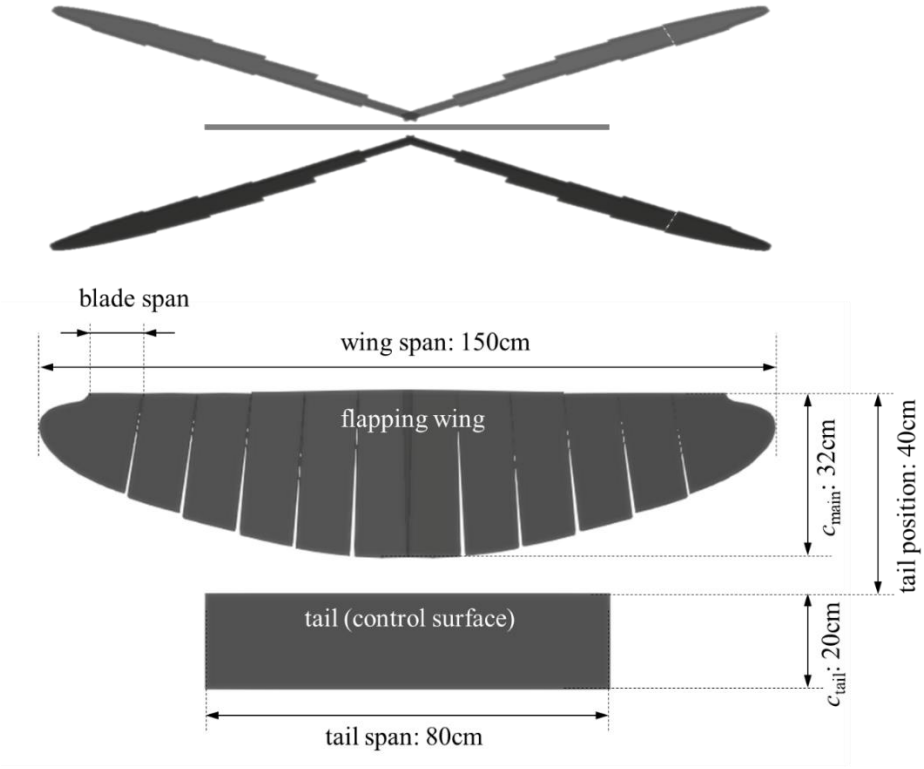

Fig. 2 Wing segmentation model in simulation

The initial flow velocity is set as zero, indicating the wings start to flap in static air condition. Post process data is acquired after 14 complete flapping cycle, when the surrounding air structure become stable among cycles. As illustrated in Fig. 1, negative *Z* direction is positive of the thrust and positive *Y* direction is positive of the control force. *X*, *Y*, *Z* can also be called as wingspan, ventral-dorsal and chord directions.

Nondimensional time t^* is utilized, wich is defined by scaling the time of each phase with the flapping period, beginning at $\phi = 0°$ when leading edges of upper and lower wings are coincide.

4. Time domain result

4.1 Flow structure analysis

The overall simulatied result of the main flapping wing wake is illustrated in Fig. 3(a). The displayed moment is $t^* = 0.7$, when the wings just passed maximum flapping angle limit, and start to clap. The t^* is selected because the flow structure is relatively obvious at this moment. It is seen the induced jet flow zone constrained between two flapping wings. The induced velocity is uneven distributed in the wake, and is seen mixing, blending with surrounding static air mass, the velocity is therefore decrease when the flow transmitting downstreams.

The high speed flow between the wings dicrease the pressure at wing surface that facing the high speed flow, which is seen in Fig. 3(b). The pressure difference between upper and lower wing surfaces generates aerodynamic force, whose *Y* components counteract each other due to flow field symmetry, and *Z* components add up to constitute the thrust.

The induced air mass distribution in the wake is further analyzed by isosurface figure in Fig. 3(c).

The isosurfaces represent v_z = 5.5m/s, the envelope air mass has higher induced speed, and is considered here as obvious induced zones. The induced air mass has a similar crescent moon shape as the wings trailing edge, and has a gap around wing root axis. The air mass induced by the current flap stroke and by the previous stroke is both seen. It indicates that the induced air mass volume doesn't drop much after transmitted downstream within one flap period, but then decrease sharply when passing further.

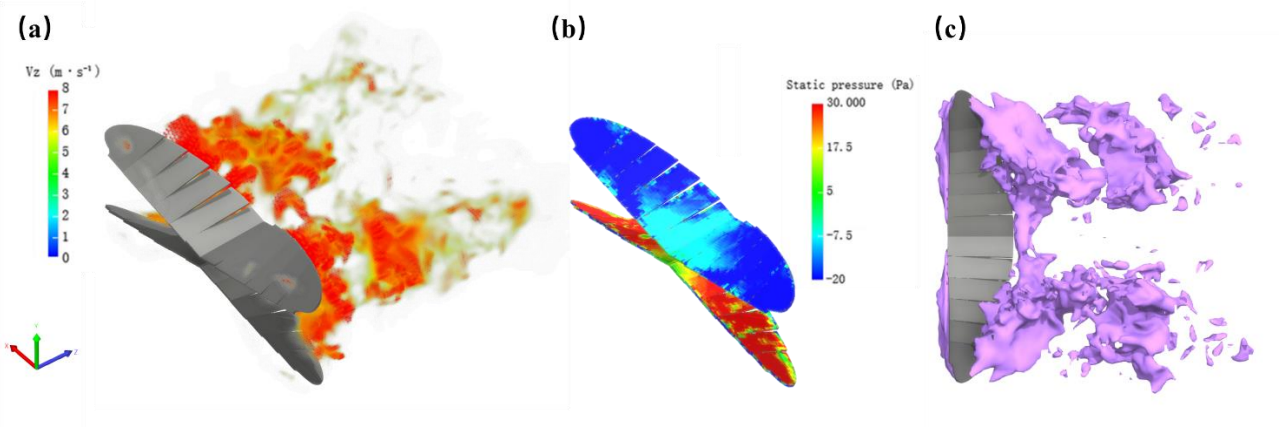

Fig. 3 (a) v_z amplitude contour, (b)pressure distribution on the wing surfaces, (c)iso surface of v_z with threshold of 5.5m/s

Flow field at a medium span *y-z* section planes *x* = 0.45m, with 5° elevator deflection are analyzed as illustrated in Fig. 4, since the flow structure is relatively obvious at this cutting plane. The arrows represent local velocity vector direction and the color represents magnitude.

At $t^* = 0$, leading edges of the upper and lower wings are parallel and the major induced red area generated by the previous cycle are seen downstream the trailing edge.

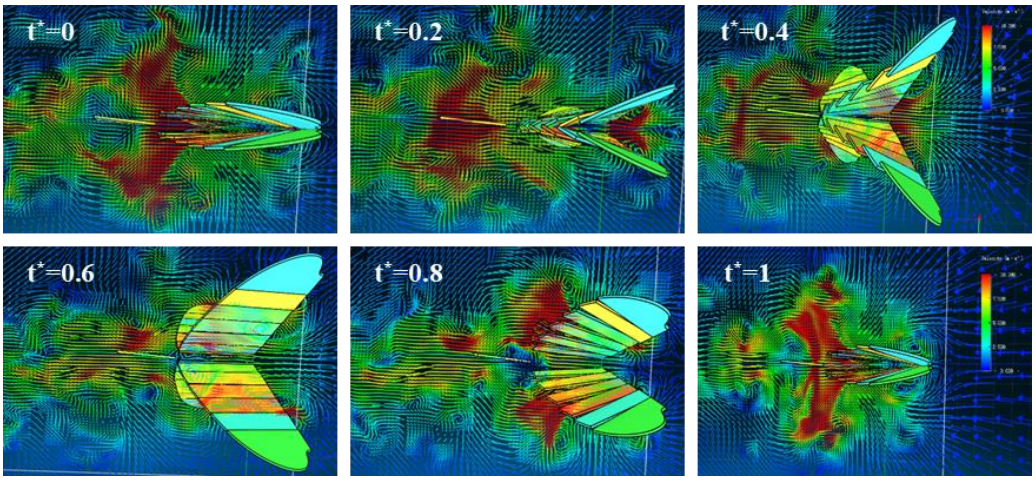

Fig. 4 Flow vectors at *y-z* section plane *x* = 0.45m, with 5° elevator deflection

At $t^* = 0.2$, the leading edges begin to peel and a strong induced zone is generated around leading edge, between upper and lower flapping wings. If we define the space between the two flapping wings as internal, and the space upper or lower the two wings as external, it can be seen that the external field attenuates and the velocity of the internal wedge-shaped area increase sharply, the overall thrust rising accordingly.

The flow field result from $t^* = 0.4$ to $t^* = 0.8$ make it clear that how the main induced area forms. It is seen that the red induced zone formed at $t^* = 0.2$ translate from the leading edge to the trailing edge, and become stronger as the two flap wings reverse flap direction and start to clap. The red

induced zone is seen passing the tail at $t^* = 0.2$, with flow direction basically coincide with *Z* positive direction, thus create an ideal flow field for tail control force generation. However, at other t^*, the flow around the tail is weak. The tail surrounding flow variation indicates that the tail control force is also periodical.

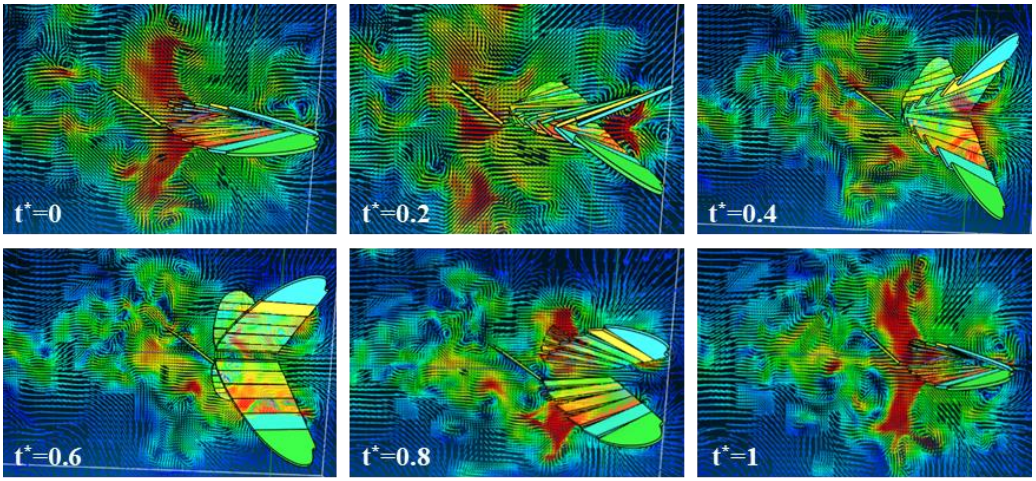

Fig. 5 Flow vectors at *y-z* section plane *x* = 0.45m, with 35° elevator deflection

Flow field on the upper and lower sides of the tail is basically symmetric at small elevator angles. Therefore, the control force is small, and is possibly submerged in the unsteady effect of eddy current. Fig.5 demonstrations the flow field under a moderate elevator angles, 35°. It is seen that there is an obvious high-speed flow zone beneath it when strong induced flow passing, which is clearly displayed at $t^* = 0.2$. Therefore, there is a large pressure difference on the upper and lower surfaces of the tail to generate considerable control force.

4.2 Aerodynamic force analysis

In addition to the flow structure, the transient control force is also obtained in the simulation. The flapping angle, transient/cycle-averaged thrust force of the flapping wing, and the control force of the tail, is compared in Fig. 6. The ornithopter weights 0.8kg and the simulated results inform that the average thrust is about 8.5N. Considering the approximate conditions of the simulation model and errors caused by unsteady flow, the result is deemed to be acceptable.

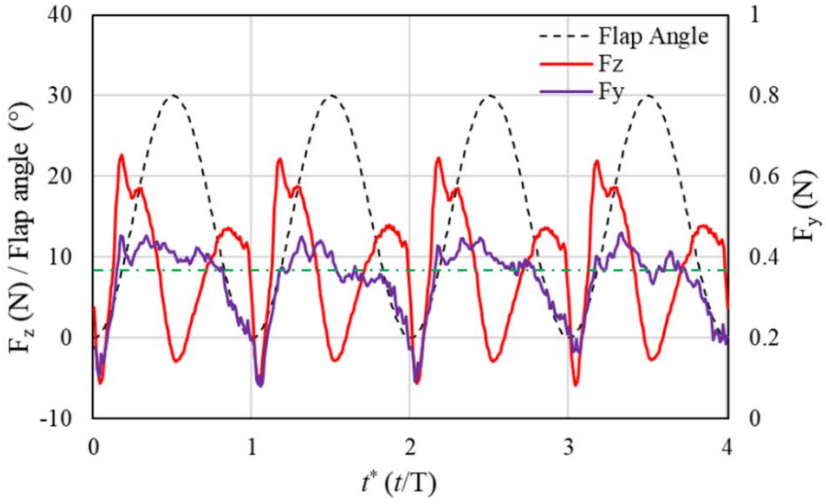

Fig. 6 Ilustration of the relationships between flapping angle, transient/cycle-averaged thrust force of the flapping wing, and the control force of the tail

It is seen from Fig. 6 that thrust force curve F_z forms two peaks within one flap cycle, corresponding to the middle of clap/peel stroke. The tail control force is proportional with the flapping wing thrust

force, which is reasonable since the induced flow velocity dominates tail control force generation.

It should be noticed that although thrust force have a remarkable drop at middle period, control force doesn't drop much at this moment. It can be seen from 3D flow structure result that even though the thrust decrease to zero around $t^* = 0.5$, the induced flow zone is not disconnected at this moment, and the flapping wings form only one induced flow zone every flap period. Therefore, it can be deduced that the tail control force curve trully should have one trough every period, when the flapping wings clap and cut off the induced flow zone.

Cycle averaged control force coefficient of the tail is illustrated in Fig. 7(a). It is seen that there is an approximate linear relationship between averaged control force and elevator angles before 40°. When tail pitch angle is larger than 40°, "stall" phenomenon occurs and a sharp decrease of tail control force is seen. It is noticed that the "stall" starts at a much larger angle than static stall angle of the airfoil, which normally between 10° and 20°. Since the flapping wing wake is highly turbulented, the tail's boundary layer should have high energy level, thus may lead to better seperation performance, similar with the function of a vortex generator on an aircraft wing. However, further researches are needed to derive a solid conclusion.

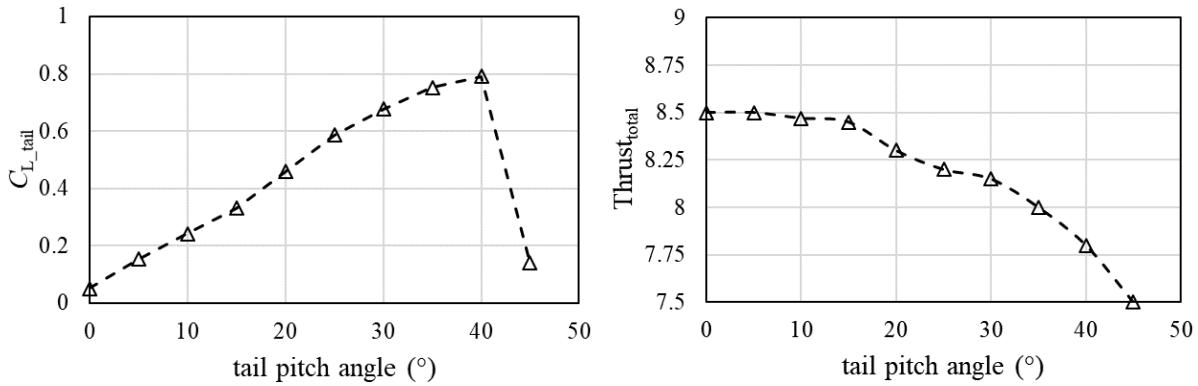

Fig. 7 (a)Cycle averaged control force coefficient of the tail, (b)Overall *Z* direction force generated by the flapping wing plus the tail

The overall *Z* direction force generated by the flapping wing plus the tail is illustrated in Fig. 7(b). The flapping wings generate *Z* negative thrust, while the tail generate *Z* positive drag. It is seen that at a small tail pitch angle lesser than 10deg, the overall thrust almost keep constant. When the tail deflection increasing and larger than 15°, the overall thrust decreases remarkably. It is reasonable since when the tail pitch angle increases, the tail's drag increases correspondingly and behave as an air break.

5. Cycle-averaged analytical model

5.1 Momentum theory based model

Although flying creatures utilized periodical varying complex tail control strategy to maximize control effect and to achieve agile flight, it is unpractical for man-made flapping wing aircraft due to steep requirements on servo bandwidth and power consumption. Therefore, existing flapping wing control studies mostly build control models based on cycle-averaged control effect. Since the actual control force varying at the same frequency of flapping, cycle-average method is valid so long as flapping frequency is an order of magnitude higher than short-period frequency.

In existing flapping wing aircraft control moddels, bernoulli's equation are most frequently used to derive the tail's control force, and the flying speed is substitude as characteristic velocity, without considering of flapping induced velocity. This method is valid during level high speed flight, but has large deviation when flgiht speed is low, especially at hovering situation. To address the hovering

control problem of Beihawk, the cycle-averaged tail aero-force model considering flapping wing induced flow velocity is analyzed in this section.

From 3D wake structure analysis as in Fig. 3, it can be deduced that the tail incoming flow velocity is maily constrained in *Z* positive direction, especially when strong induced flow passing. Since the transient aerodynamic force generated by the tail is related to native incoming flow velocity, if cycle-averaged flow velocity can be derived, the control force generaged by the tail is expressed as

$$F_y = \frac{1}{2}\rho v_z^{\,2} S_{tail} C_{tail} . \tag{2}$$

The momentum theory describes a mathematical model, actuator disc, for propulsion devices, such as a propeller. This theory is a widely used as a steady method to study the relationships between velocity, pressure, force, power and efficiency, and also be transplanted for flapping wing study, as illustrated in Fig. 8. The actuator disc model of flapping wings is consist of two fan areas, where the flapping wing leading edge swept, constrains on the flapping stroke plane. Based on momentum theory, the airflow is accelerated by the actuator disc. Thus, the flow tunnel section constricting while transmitting downstream, and the flow speed increasing correspondingly, until the static pressure balanced with the surrounding air mass.

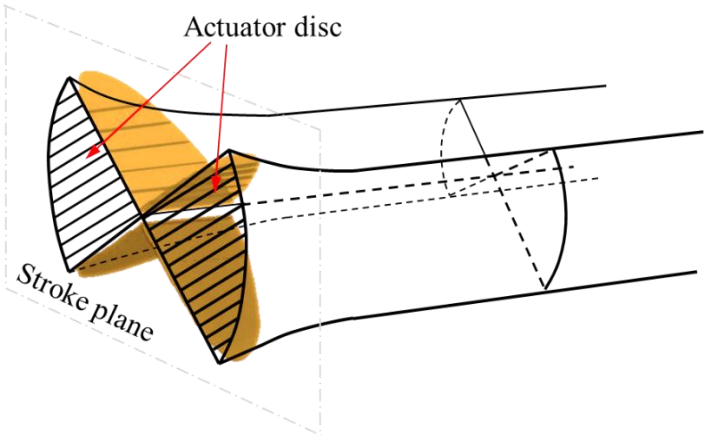

Fig. 8 The actuator disc model of flapping wings

The speed of the actuator induced flow can be derived from the disc thrust generation, expressed as

$$\omega(0) = 0.5\left[\sqrt{V_0^{\,2} + \frac{2T}{\rho\pi R^2}} - V_0\right]. \tag{3}$$

It is obvious that in hovering status, v_0 is zero. With a consumption that the flow tube isolate the flow inner and outer, the downstream speed will finally approach $2v_0$. The theoretical downstream speed distribution is expressed as

$$\omega(s) = \omega(0)\left[1 + \frac{s/R}{\sqrt{1+(s/R)^2}}\right]. \tag{4}$$

Plug Eq. (3) into Eq. (4), cycle-averaged tail control force can be derived.

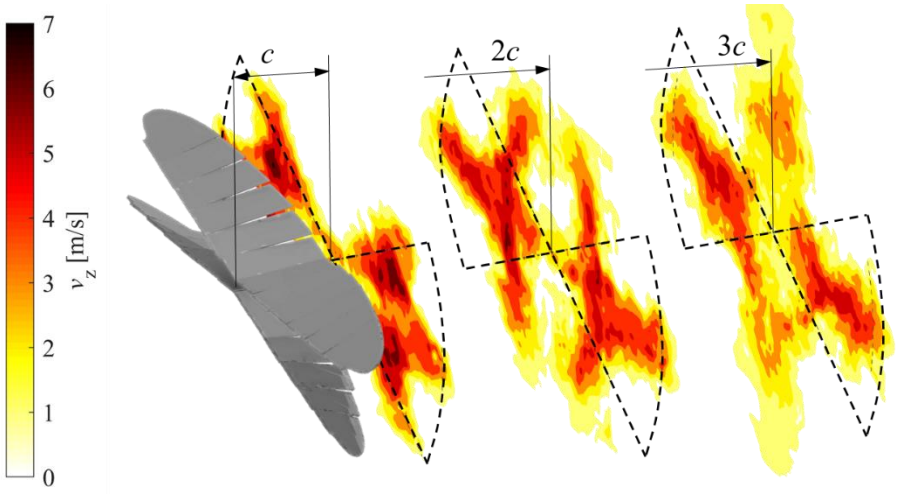

Fig. 9 Cycle-averaged velocity fields on different cross sections

5.2 Application and Validation

However, the actuator disc model is a rough approximation, the acutal wake structure is more complex. To address the deviation of this method, cycle-averaged velocity field is studied as illustrated in Fig. 9. The cycle-averaged *Z* positive velocity field on cross sections at *Z*=1*C*, 2*C*, 3*C* are constructed based on simulational data. Within one flapping cycle, 40 frames with the same interval are utilized to derive cycle-average result. Dashed lines represent the limiting position of the leading edge of the flapping wings.

It can be seen at 1*C* section, the high speed induced zone nicely overlap the wing swept fan area. The velocity peak zones locates at medial span-wise and middle flapping angle position. When the flow transmitting downstream, the velocity peak zone is seen moving towards the area where the wings clap and peel, also it is the zone where the tail installed. The other branch of the obvious induced zone is expand towards the gap between the two fan areas, perpandicular to the line where the wings clap. But the velocity amplitude is relatively weaker. At 3*C* section, the induced zone shape deviate from the wing swept fan area, but the fan area still contain the main induced flow component.

Next, the averaged velocity in the fan areas is utilized to derive tail control force based on Eq. (2). The theoretical versus simulated results are presented in Fig. 10. It is seen that the trend of theoretical curve agree with simulated data. Maximal control force error is 0.07N, less than 12% force peak value.

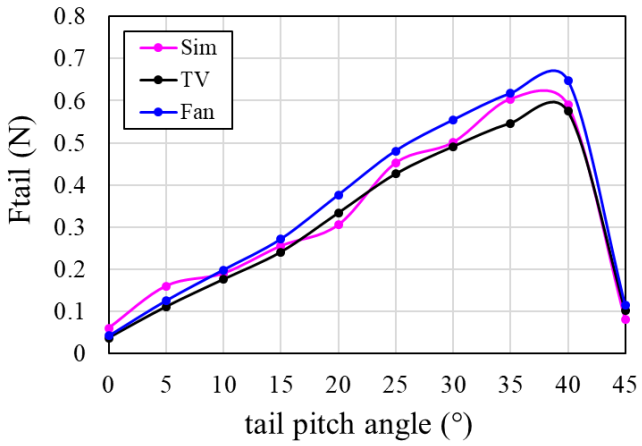

Fig. 10 Theoretical versus simulated tail control results at different tail pitch angle

In order to validate the relationship between thrust force and induced velocity in Eq. (3, 4), theoretical v_{tail} value based on momentum theory is compaired with simulated v_{tail} value based on above

mentioned fan area method, at differnent *Z* positive positions. Flapping wing thrust is adjusted through the changing of flapping frequency from 4-10Hz. Different with propellers, flapping wings have relative large axial length, which means the actuator disc has a considerable thickness. A problem arise that whether the flapping wing leading edge stroke plane should be considered as the disc plane, or the trailing edge. To investigate this, both assumption are tested. The result is that assuming leading edge stroke plane to be the actuator disc plane derives much better fitting result with simulated data. The overall fitting result based on this assumption is illustrated in Fig. 11.

It can be seen that with frequency increasing, the theoretical $\omega(0)$ increases from 1.3m/s to 3.1m/s, with hyper linear pattern. With the increment of *Z*, theoretical $\omega(z)$ continually increasing and approaching $2\,\omega(0)$. Simulated data is collected from *C* = 1, i.e., the trailing edge plane. It can be seen that within *Z* = *C* to 1.5*C*, the simulated $\omega(z)$ agree with theoretical prediction well. When *Z* is larger than 1.5*C*, simulated $\omega(z)$ start to decrease, theoretical deviation become larger. Thus, it can be concluded that momentum theory successfully predict the induced velocity near the actuator disc plane. Within a short distance downstream the actuator disc, the induced flow is continue accelerating as momentum theory predicted. When the flow go further downstream, the flow mixed up with surrounding static air, the velocity decrease quicly. It should be noticed that at 4Hz, the simulated w(z) start to decrease with *Z* right behind the trailing edge. This is reasonable since at a lower flapping frequency, the induced flow is weaker, and mixing with surrounding static air sooner.

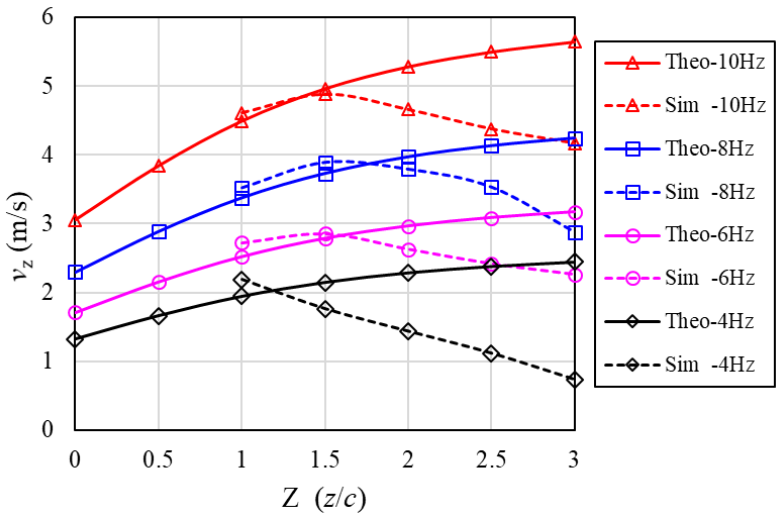

Fig. 11 simulated results vs theoretical results of flapping wing induced velocity

During static hovering, the lift generated by flapping wing balance the weight. Therefore, the induced velocity at 1.5*C*, where the tail installed, can be calculated based on Eq. (3, 4). The control model of the tail is then aquired based on Eq. (2). In actual flying missions, the aircraft need to conduct hovering based maneuvers or flying against gust, thus require larger thrust generation, up to 1.5 times of weight. In this case, assumption of *T* = *W* will generate considerable errors. For more precise flight control, a further research connecting relationships between flapping wing kinematics and thrust is needed. Integration of these method will derive more general tail modelling method, adapting hovering, level flight and transition.

6. Conclusion

The control features of X-shape flapping wing aircraft tail that installed within the main wing induced flow field is studied. Numerical method is utilized for flow structure and aerodynamic field feature analysis. It is seen from flow structure result that a pair of strong induced air mass generated during each flap cycle. The tail control force reach peak value when the induced air mass passing the tail,

the control force curve therefore has one peak within one flap cycle while the flapping wing thrust force curve have two. The cycle-averaged tail control force is found increasing linearly with pitch angle, and doesn't show stall features until the pitch angle reaches 40°.

Actuator disc theory is utilized for analytical method construction. Previously proposed fan-shape-section flow tube assumption of flapping wings is adopted. Simulated result indicate the tail cycle-average control force can be derived base on the cycle-averaged velocity within the fan shape and simple Bernoulli equation. The theoretical actuator disc induced velocity increases when the flow going downstream from the trailing edge of the flapping wings to 0.5 chord length downstream the trailing edge, which agrees well with simulated data. When the wake transmitting further downstream, the simulated induced velocity display a sharp decrease while theoretical result continue increasing and approaching two times the velocity at actuator disc. Compared with propeller's wake, it is seen flapping wing wake dissipate faster, may attributed to it's high turbulence nature.

Since the tail of the considered aircraft is installed closer than 0.5 chord length from flapping wing trailing edge, the cycle averaged induced velocity can be derived by disc actuator theory, and the cycle-averaged control force of the tail is therefore derived. This analytical method for tail control feature estimating has potential utilization in flapping wing tail design, especially when aircrafts fly at low airspeed or hovering, and have a high control requirement for the tail.

7. Copyright Statement

Reference

[1] W. Shyy, H. Aono, C.-k. Kang, and H. Liu, An introduction to flapping wing aerodynamics: Cambridge University Press, 2013.

[2] W. Send, M. Fischer, K. Jebens, R. Mugrauer, A. Nagarathinam, and F. Scharstein, "Artificial hinged-wing bird with active torsion and partially linear kinematics." pp. 23-28.

[3] T. N. Pornsin-Sirirak, Y.-C. Tai, C.-M. Ho, and M. Keennon, "Microbat: A palm-sized electrically powered ornithopter." pp. 14-17.

[4] A. M. Lippisch, "Man Powered Flight in 1929," Journal of the Royal Aeronautical Society, vol. 64, no. 595, pp. 395-398, 1960.

[5] J. D. DeLaurier, "The development and testing of a full-scale piloted ornithopter," Canadian aeronautics and space journal, vol. 45, no. 2, pp. 72-82, 1999.

[6] G. K. Taylor, R. L. Nudds, and A. L. Thomas, "Flying and swimming animals cruise at a Strouhal number tuned for high power efficiency," Nature, vol. 425, no. 6959, pp. 707-711, 2003.

[7] J. D. Delaurier, "Ornithopter wing design," Canadian Aeronautics & Space Journal, 1999.

[8] M. Sun, "Insect flight dynamics: Stability and control," Rev.mod.phys, vol. 86, no. 2, pp. 615-646, 2014.

[9] S. Heathcote, and I. Gursul, "Flexible flapping airfoil propulsion at low Reynolds numbers," AIAA journal, vol. 45, no. 5, pp. 1066-1079, 2007.

[10] J. D. DeLaurier, "An aerodynamic model for flapping-wing flight," The Aeronautical Journal (1968), vol. 97, no. 964, pp. 125-130, 1993.

[11] X. Deng, L. Schenato, W. C. Wu, and S. S. Sastry, "Flapping flight for biomimetic robotic insects: part I-system modeling," IEEE Transactions on Robotics, vol. 22, no. 4, pp. 776-788, 2006.

[12] M. H. Dickinson, F.-O. Lehmann, and S. P. Sane, "Wing Rotation and the Aerodynamic Basis of Insect Flight," Science (New York, N.Y.), vol. 284, no. 5422, pp. 1954-60, 1999.

[13] H. Mahjoubi, and K. Byl, "Dynamics of insect-inspired flapping-wing MAVs: Multibody modeling

and flight control simulations." pp. 3089-3095.

[14] X. Deng, L. Schenato, and S. S. Sastry, “Flapping flight for biomimetic robotic insects: Part II-flight control design,” IEEE Transactions on Robotics, vol. 22, no. 4, pp. 789-803, 2006.

[15] S.-J. Chung, and M. Dorothy, “Neurobiologically inspired control of engineered flapping flight,” Journal of guidance, control, and dynamics, vol. 33, no. 2, pp. 440-453, 2010.

[16] P. Chirarattananon, K. Y. Ma, and R. J. Wood, "Adaptive control for takeoff, hovering, and landing of a robotic fly." pp. 3808-3815.

[17] D. D. Chin, and D. Lentink, “Flapping wing aerodynamics: from insects to vertebrates,” Journal of Experimental Biology, vol. 219, no. 7, pp. 920-932, 2016.

[18] C. Ellington, “The aerodynamics of hovering insect flight. 5. A vortex theory,” Philosophical Transactions of the Royal Society of London Series B-Biological Sciences, vol. 305, no. 1122, pp. 115-144, 1984.

[19] S. P. Sane, “The aerodynamics of insect flight,” The journal of experimental Biology, vol. 206, no. 23, pp. 4191-4208, 2003.

[20] D. Mackenzie, "A flapping of wings," American Association for the Advancement of Science, 2012.

[21] P. Zdunich, D. Bilyk, M. MacMaster, D. Loewen, J. DeLaurier, R. Kornbluh, T. Low, S. Stanford, and D. Holeman, “Development and testing of the mentor flapping-wing micro air vehicle,” Journal of Aircraft, vol. 44, no. 5, pp. 1701-1711, 2007.

[22] G. De Croon, M. Perçin, B. Remes, R. Ruijsink, and C. De Wagter, “The delfly,” Dordrecht: Springer Netherlands. doi, vol. 10, pp. 978-94, 2016.

[23] L. Long, and T. Fritz, “Object-Oriented Unsteady Vortex Lattice Method for Flapping Flight,” Journal of Aircraft, vol. 41, no. 41, pp. 1275-1290, 2004.

[24] Z. Jiao, L. Zhao, Y. Shang, and X. Sun, “Generic Analytical Thrust-Force Model for Flapping Wings,” AIAA Journal, pp. 1-13, 2017.